Journal of Sol-Gel Science and Technology 23, 253–263, 2002

Characterization of Hollow Chemical Garden Fibers from Metal Salts and Water Glass

D. BALKÖSE* AND F. ÖZKAN
Izmir Institute of Technology, Faculty of Engineering, Department of Chemical Engineering, Urla İzmir, Turkey
dbalkose@likya.iyte.edu.tr

U. KÖKTÜRK
9 September University, Faculty of Engineering, Department of Mining Engineering, 35100 Bornova İzmir, Turkey

S. ULUTAN
Ege University, Engineering Faculty, Department of Chemical Engineering, 35100 Bornova-İzmir, Turkey

S. ÜLKÜ
Izmir Institute of Technology, Faculty of Engineering, Department of Chemical Engineering, Urla İzmir, Turkey

G. NİŞLİ
Ege University, Science Faculty, Chemistry Department, 35100 Bornova İzmir, Turkey

Received July 27, 2000; Accepted September 7, 2001

Abstract. Hollow fibers formed from water glass and metal salts of IIA(Ca), VIIB(Fe, Co, Ni) and IB(Cu) groups were characterised in this study. Fragile fibres obtained herein broke down into small pieces during isolation and drying. Quantitative information about morphology, chemical composition and surface structure of the fibres were obtained. The diameter and wall thickness of the fibers were around 50 μ and 3 μ. respectively. They had particulate inner and smooth outer surfaces. Fibers had variable composition with metal (II) oxide/SiO_2 ratio in the range 0.31 to 1.02. While group VIIB metal (II) fibres were amorphous, group IIA and IB metal (II) fibres were partially crystalline All the fibres had pores both in micro pore and meso pore region. The B.E.T surface area from N_2 adsorption data was in the range of 10–249 $m^3\ g^{-1}$ and 8–176 $m^2\ g^{-1}$ from Langmuir and B.E.T models respectively.

Keywords: chemical garden, water glass, metal silicates, nitrogen adsorption, water vapour adsorption, inductively coupled plasma

Introduction

Hollow fibers have practical aplications in membrane separations, catalytic reactions and controlled flow of the liquids. It is well known that capillary fibers so called as "chemical garden" form when metal salts are introduced into water glass. The mechanism of formation is explained in terms of the semipermeable membrane formation, osmotic pressure, diffusion and viscous flow [1, 2]. Since the dissolved salt concentration is greater in the space between crystal and the membrane than in the surrounding solution water diffuses

*To whom all correspondence should be addressed.

into this space. The osmotic pressure thus increases and the membrane expands and bursts. The hole thus formed is immediately filled by metal salt solution. The salt concentration is lowest at the highest point of the membrane, so that the latter normally bursts here and the fibers grow upwords [2]. Since hydrogen and hydroxyl ions diffuse rapidly, silica gel is formed on the silicate side and metal hydroxide on the metal salt side [3]. Amorphous precipitate formation was reported when water glass was reacted with metal ions in aqueous solutions [3]. Various growth morphologies obtained in silicate garden were studied by Coatman et al. [4]. Hollow fibers with globular morphology having amorphous structure were formed from metal salts and water glass.

Hierarchical nanostructure involving approximately 44 nm diameter tubes in aluminum silicate fibers were recently reported [5]. Periodic array of microtubules 4.4 μm in diameter formed the macroscopic fibers in 0.16 mm diameter. NMR and ESCA studies of silicate gardens showed that they were Bronsted acids [6]. Filamentous growth during drying of SiO_2 gels prepared from TEOS and NH_3 was also reported [7]. Meso porous Molecular Sieves MCM-41 with hollow tubular morphology were obtained using surface active agents as templating materials [8]. The length of the tubes were at the size of surface active agent micelles. Valtchev et al. [9] characterized hollow fibers of silicalite I which were obtained by calcining silica precipitated on carbon fiber templates. Silica hollow fibers were obtained from organic precursers such as hydridopolysilazanes. Extrusion, treating HCl followed by water vapor treatment and pyrolysis in two steps at 600–1000°C and compaction at 1200–2000°C are the processes used in their production [10]. Microporous polypropylene hollow fibers filled with adsorbent particles have been successfully used separating hydrogen from nitrogen and carbondioxide [11]. Preliminary results of hollow fiber formation from water glass and metal salts and characterization of dried fibers study were reported by Balköse et al. [12].

Probable reactions that occur when metal (II), M(II) salts are added to water glass are as the following.

Metathesis reaction:

$$Na_2O{\cdot}xSiO_2 + M^{2+} \rightarrow MO{\cdot}xSiO_2 + 2Na^+ \quad (1)$$

Hydroxide precipitation:

$$M^{2+} + 2OH^- \rightarrow M(OH)_2 \quad (2)$$

Hydroxide polymerization:

$$M(OH)_2 \rightarrow -(-M-O-)_x- + xH_2O \quad (3)$$

Silica precipitation:

$$Na_2O{\cdot}xSiO_2 + 2H^+ \rightarrow xSiO_2 + H_2O + 2Na^+ \quad (4)$$

Oxidation of M^{2+} to higher oxidation states with the dissolved oxygen:

$$M^{2+} \rightarrow M^{3+} + e^- \quad (5)$$

Since catalytic effect of silica on oxidation of ferrous ions to ferric ions by the dissolved oxygen in water is known [13], oxidation of other M(II) ions is also expected.

The aim of this study is to characterize fibers formed from water glass and metal salts rather than to explain their mechanism of formation. Salts of metals from groups IIA, VIIB and IB of the periodic table were chosen to observe their behavior in fiber formation and to determine their effect on pore structure of the fibers.

Hollow fibers from M(II) salts and water glass were separated, washed and dried. They were analysed by inductively coupled plasma (ICP) and characterised by scanning electron microscopy (SEM) for their morphology, infrared (IR) spectroscopy for functional groups, X-ray diffraction for crystal structure, thermal gravimetric analysis (TGA) and differential scanning calorimeter (DSC) for water release, volumetric adsorption of nitrogen and water vapour for their pore structure.

Experimental

Water glass from Tunçtaş with 5.6% Na_2O and 17.9% SiO_2 was diluted five times of its initial volume. Soluble $CaCl_2$, $FeSO_4{\cdot}7H_2O$, $CuSO_4{\cdot}5H_2O$, $CoCl_2{\cdot}6H_2O$ and $NiCl_2{\cdot}6H_2O$ crystals of 1–3 mm particle size were added to water glass one at each time. The behavior of fiber formation was observed up to one year. The hollow fibers formed were separated by decantation after one week and washed with distilled water till pH decreased from 13.5 to 10 and they were dried at 25°C in air.

The scanning electron micrographs of the gold coated fibers were obtained with Jeol scanning electron microscope.

The chemical analysis of the fibers were made by dissolving the residue in aqua regia after HF treatment of the fibers and SiF_4 evaporation till dryness. The solutions were analyzed using Varian ICP-AES Liberty

Series II for Al, Ca, Co, Cu, Fe, K, Mg, Na, Ni and Si elements.

The IR spectra of the dried fibers were taken using KBr disc technique in the transmission mode with Shimadzu IR 470 spectrometer. The IR spectra of $CaCO_3$ with different concentrations in KBr were also taken to determine the $CaCO_3$ content of the fibers. The x-ray powder diffraction diagrams of the fibers were obtained by using Jeol JSDX-100S X-ray diffractometer. The fibers were equilibriated with 75% relative humidity air at 25°C for TGA and DSC analysis. TGA curves of the fibers were taken by heating the fibers from 25–1000°C at 10°C/min rate using Shimadzu TGA51. DSC curves of the fibers were taken by heating the fibers from 25 to 300°C with 10°C/min rate using Setaram DSC92.

True density of the fibers were determined by water pycnometry by measuring the volume of the water displaced by the samples after removing the air in the pores by vacuum application to water and fiber mixture.

Adsorption and desorption isotherms for N_2 at -196°C and for H_2O at 25°C were determined by static dosing method using Omnisorp 100 CX volumetric adsorption instrument. The samples were outgassed at 10^{-4} mbar pressure at 150°C for 2 hours before each adsorption experiment. The desorption was recorded down to relative pressure of 0.4.

Results and Discussion

When metal salts were dropped in diluted water glass a gelatinous membrane forms around the salts according to reactions (1) to (4). The membrane allows 0.28 nm sized water molecules to pass through, but not permit hydrated metal cations of 0.4 nm size. When the osmotic pressure created due to concentration difference between two sides exceeded the tensile strength of the membrane, the membrane bursts in form of pinholes and the salt solution inside the membrane is ejected in water glass and immediate gelatinous precipitate formation occurred. By repetition of this process many times chemical garden fibers formed. All the fibers had tubular morphology and inside of the tubes were filled with salt solution when they were formed. The isolation of the fibers from the solution was accomplished by separating the water glass and gelatinous silica from higher density fibers by decantation. Then the fibers were washed for purification with distilled water, were filtered and dried. The fibers were fragile and become partially pulverized during filtration and drying. The attempt to strengthen the fibers by aging for long times were failed due to complete hydrogel formation outside the fibers making separation of fibers and the hydrogel impossible. Since their exact stoichiometric composition is not known, fibers are going to be called in the text with the name of the cation used in their preparation.

The colors of the Ca(II), Fe(II), Co(II), Ni(II) and Cu(II) fibers were white, light green, dark blue, green and light blue respectively when they were first formed. Fe(II) fibers became brown on standing in water glass for one week due to oxidation of Fe(II) to Fe(III) with the dissolved oxygen as expected [13].

All the fibers formed in water glass had tubular morphology as seen in representative micrographs in Fig. 1. Longitudinal section from Fe(II) hollow fiber in Fig. 1(c) showed the membrane wall, smooth external surface and particulate inner surface of Fe(II) fibers. The diameter and wall thickness of the fibers were around 50 μ and 3 μ respectively. Coatman et al. [4] also reported formation of hollow Fe(II) fibers having very close dimensions of the fibers of the present study. They were 40 μ in diameter and 4 μ in wall thickness [4].

The inner surface of the Ca(II), Fe(II) and Co(II) fibers consisted of granules with 2.9, 0.5 and 1 μ average diameter as seen in Fig. 1(b), (d) and (f) respectively. It was thought that inner surface of the fibres were metal hydroxides or oxides and their smooth outer surface was the hydrated metal silicate and silica gel [5]. Three different layers distinguishable in cross section of the fibers seen in Fig. 1(c) and (f) could be attributed to silica, metal silicate and metal oxide or hydroxide from outside to inwards respectively.

Composition of the Fibers

The composition of the fibers reported as mol of oxides per mol of SiO_2 in Table 1 indicated they were not stoichiometrically equivalent compounds. They all differed from each other in metal (II) oxide/SiO_2 ratio. If only Na^+ ions were exchanged with other cations the metal (II) oxide/SiO_2 ratio would be the same, 0.31, with that of the starting water glass. The metal (II) oxide/SiO_2 ratio of the fibers were in the range 0.31 to 1.02 . All of the fibers had also Na_2O and K_2O in appreciable quantities (0.08–0.22 mol/mol SiO_2) besides the oxides of the salts used in their synthesis. This brought the probability of insoluble double salt formation or sodium silicate occlusion [14] in the fibers under consideration.

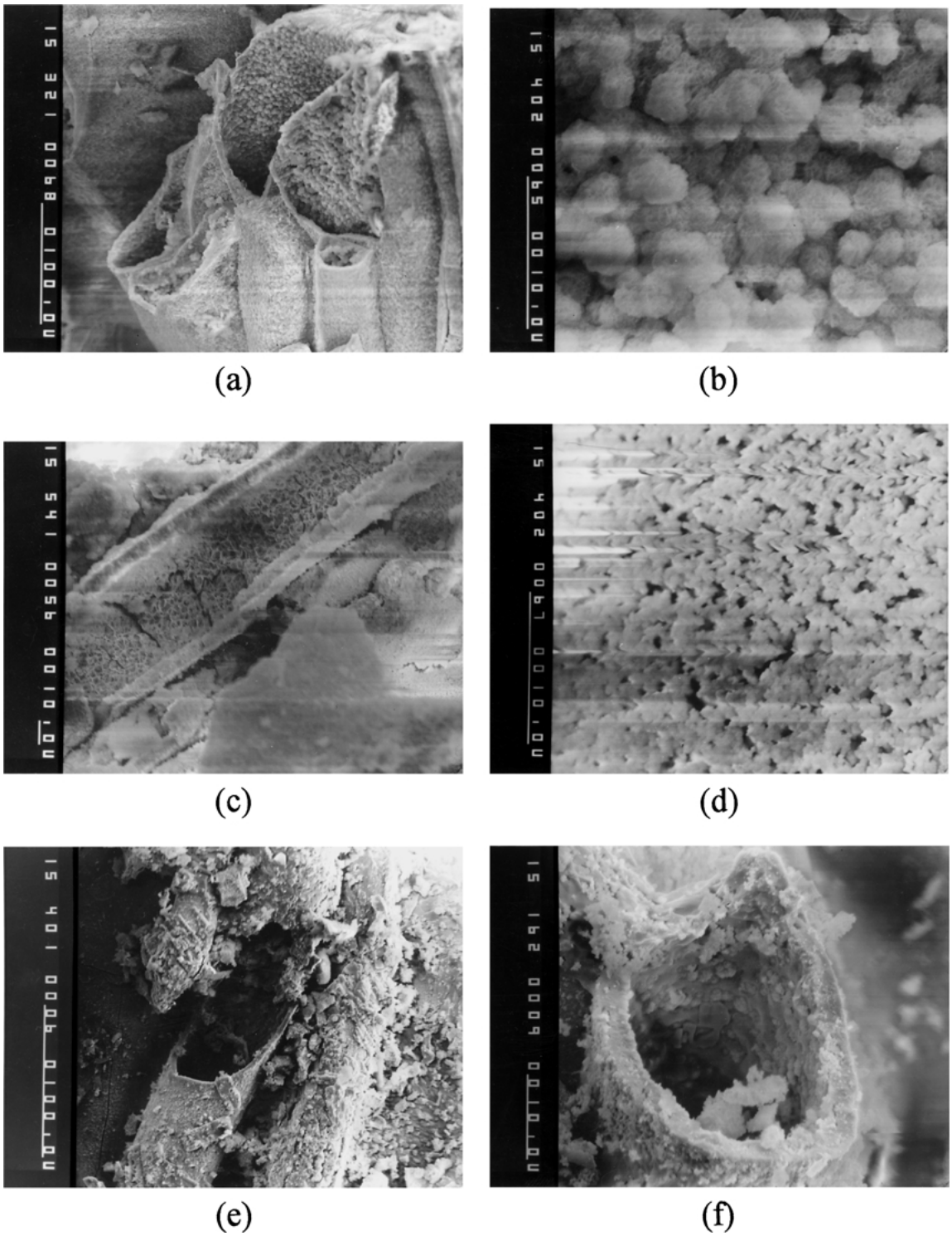

Figure 1. Electron micrographs of chemical garden fibers (a) Ca(II) fiber with 320x magnification, (b) inner surface of Ca(II) fiber with 4000x magnification, (c) Fe(II) fiber with 400x magnification (d) inner surface of Fe(II) fiber with 4000x magnification (e) Co(II) fiber with 400x magnification, (f) Co(II) fiber with 1600x magnification.

Table 1. Molar Composition of hollow fibers, mol metal oxide/molSiO_2.

	Fiber type				
Composition	Ca(II)	Fe(II)	Co(II)	Ni(II)	Cu(II)
Al_2O_3	0.04	0.03	0.02	0.03	0.02
CaO	0.31	0.01	0.00	0.01	0.01
CoO	0.00	0.00	0.65	0.01	0.00
CuO	0.00	0.00	0.00	0.00	0.46
FeO	0.00	1.06	0.00	0.00	0.01
K_2O	0.03	0.05	0.05	0.05	0.02
MgO	0.00	0.00	0.00	0.01	0.01
Na_2O	0.22	0.18	0.20	0.08	0.08
NiO	0.00	0.00	0.01	0.71	0.00

Table 2. Weight % of different types of water and volatile gases and enthalpy for evaporation of free water and slightly bound water from the fibers.

	Fiber type				
Property	Ca(II)	Fe(II)	Co(II)	Ni(II)	Cu(II)
% Free water (evaporated up to 100°C)	5.0	5.5	9.2	9.4	4.8
% slightly bound water or water in mesopores (evaporated in the range 100–200°C)	5.1	5.3	3.7	6.5	6.1
Strongly bound water (evaporated in the range 200–600°C)	10.1	0.7	1.4	2.4	2.2
Evolved gases as CO_2 or SO_3 (600–1000°C)	3.0	0.8	4.8	1.0	5.4
ΔH, J/g fiber	233	336	237	293	158

Thermal Analysis

TGA analysis of the fibers indicated they lost 7.6–15.9% of their mass up to 200°C and 12.3–23.2% of their mass up to 1000°C as seen in Fig. 2 and Table 2. Fibers contained free water (4.8–9.4%), slightly bound water (3.7–6.5), and strongly bound water (0.7–10.1%) that evaporated up to 100°C, in the range 100–200°C and 200–600°C respectively [13]. Gases evolved in the range 600–1000°C (0.8–5.4%) were due to CO_2 and SO_3 gases formed from carbonate and sulfate ions. The derivative TGA curves of the samples in Fig. 3 and DSC curves in Fig. 4 were very similar to each other. The chemically bound water was removed from Ca(II) fibers at 500–600°C, from Co(II) fibers at 180–275°C and from Ni(II) fibers at 275–400°C as seen in their

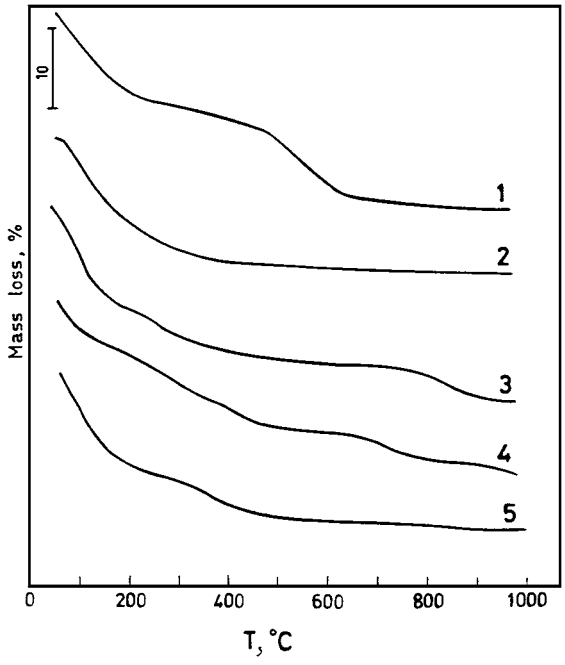

Figure 2. TGA curves of the fibers 1. Ca(II), 2. Fe(II), 3. Co(II), 4.Ni(II), 5. Cu(II) fibers.

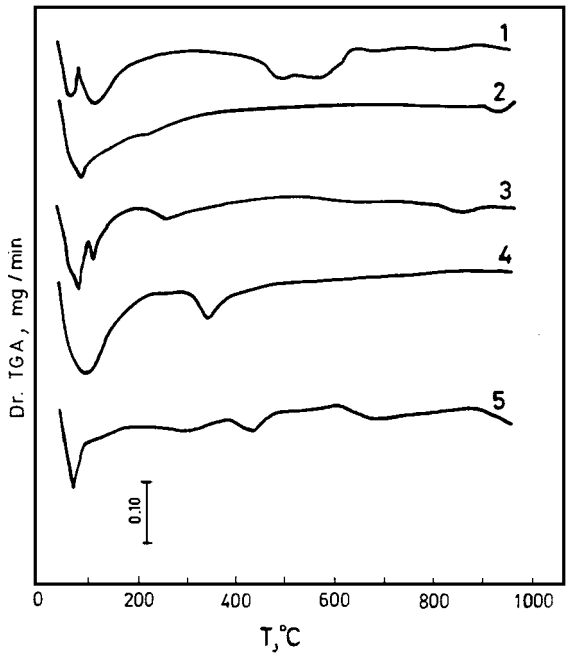

Figure 3. Derivative TGA curves of the fibers 1. Ca(II), 2. Fe(II), 3. Co(II), 4.Ni(II), 5. Cu(II) fibers.

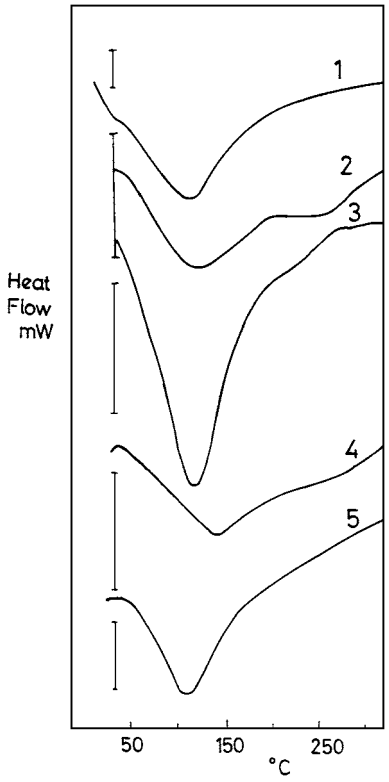

Figure 4. DSC curves for 1. Ca(II), 2. Fe(II), 3. Co(II), 4.Ni(II), 5. Cu(II) fibers. Vertical lines on Y axis represent 5 mW.

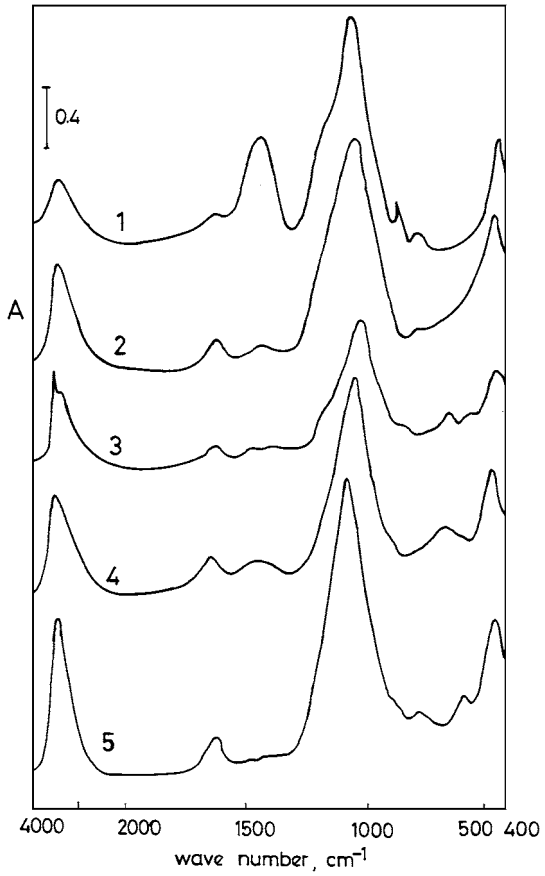

Figure 5. IR spectrum of 1. Ca(II), 2. Fe(II), 3. Co(II), 4. Ni(II), 5. Cu(II) fibers.

derivative TGA curves in Fig. 3. The endothermic large peaks in DSC curves of the fibers in Fig. 4 were integrated to find the energy required for this process. 158–336 J/g energy was absorbed as reported in Table 1, due to mainly evaporation of free water and slightly bound water [15] or water in the mesopores of the fibers [16].

IR Analysis

The IR spectra of the fibers dried at 25°C in Fig. 5 showed they all had H_2O molecules and Si-O-Si groups. The streching and bending vibration of H_2O are seen at 3400 cm^{-1} and 1600 cm^{-1} respectively. Co(II) fibers had vibrations due to isolated OH groups on their surface at 3700 cm^{-1}. Si-O-Si asymmetric and symmetric streching vibrations at 1040–1090 and 780 cm^{-1} and bending vibration at 450 cm^{-1} were observed for all the samples. No Si-OH groups were detected by IR spectroscopy since there was no peak at 960 cm^{-1} in any of the IR spectrum. While the Si-O-Si stretching vibrations are at 1040–1090 cm^{-1} for VIIA group metal ions, it is at 1090 cm^{-1} for IIA and IB metal ions. The vibration of Si-O-Si groups shifted to lower wave numbers due to increase in mass with coordination between VIIA cations and oxygens of the $SiO_4^=$ tetrahedra. All the fibers had $CO_3^=$ groups which had asymmetric stretch and symmetric bend vibrations at 1420 and 780 cm^{-1} respectively [17]. The source of $CO_3^=$ groups in the fibers was mainly water glass, which was obtained by reaction of sand and soda. CO_2 absorption from air during drying the fibers having pH value 10 is another source for $CO_3^=$ formation. Maximum $CO_3^=$ content was observed for Ca(II) fibers, since the absorbance at 1420 cm^{-1} was highest for Ca(II) fiber compared to the others. Quantitative analysis of $CO_3^=$ content by IR spectroscopy showed an equivalent of 7% $CaCO_3$ was present in Ca(II) fibers. The presence of a small amount of the sulfate ions in fibers prepared from sulfate salts were indicated by a peak around 620 cm^{-1} in their spectra [17]. It was not possible to remove salts

thoroughly from the fibers by washing them with water contrary to the expectations.

X-ray Diffraction

Water glass used in this study was an oligomeric sodium silicate with average degree of polymerization of six [18]. When it reacts with metal salts sodium ion exchanges with the cation of the salt. The arrangement of metal silicates which have six repeat units into a crystal form is difficult. Formation of amorphous precipitates occurs when salt solutions and water glass are mixed [3]. On the other hand when metal salts are added to water glass ordered structures may form. Indeed crystalline peaks in the x-ray diffraction diagrams of Ca(II) and Cu(II) were observed in Fig. 6. Fibers with Co(II), Fe(II) and Ni(II) were amorphous or they had very small crystals causing line broadening and overlapping. The X-ray diffraction diagram of Ca(II) fibers indicated presence of $CaO{\cdot}SiO_2{\cdot}H_2O$, $CaCO_3$ and $Na_2O.8CaO{\cdot}5SiO_2{\cdot}7H_2O$(19). The peaks at 0.28, 0.249 and 0.206 nm with 2θ values 35.52, 40.07 and 48.90 degrees respectively were attributed to $CaO{\cdot}SiO_2{\cdot}H_2O$ and the peak at 0.281 nm ($2\theta = 35.52^\circ$) was attributed to $CaCO_3$. The peaks at $2\theta = 29.4^\circ$ and 50° corresponding to d values of 0.304 and 0.182 nm could be due to presence of the hydrated double salt $Na_2O.8CaO{\cdot}5SiO_2{\cdot}7H_2O$. Crystalline order was also observed for Cu(II) fibers. The peaks at 0.248 nm ($2\theta = 35.8^\circ$) and 0.388 nm ($2\theta = 22.8^\circ$) were due to $CuSO_4{\cdot}H_2O$, the peak at 0.388($2\theta = 22.8^\circ$) nm was due to $CuSO_4{\cdot}3H_2O$ and the peak at 0.26 nm ($2\theta = 33.5^\circ$) was attributed to $CuSiO_3{\cdot}H_2O$. The peaks at 2θ values 24.7, 33.4 and 35.7 degrees corresponding to 0.36, 0.26 and 0.25 nm d values could be due to the presence of double salt Na_2CuSO_4 [19].

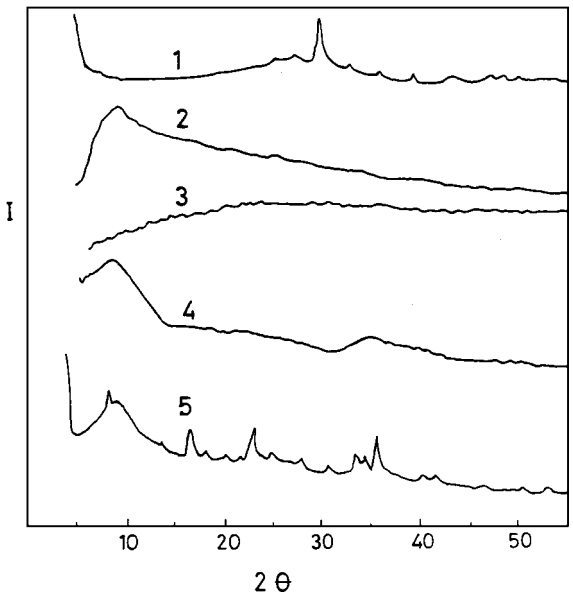

Figure 6. X-ray diffraction diagram of 1. Ca(II), 2. Fe(II), 3. Co(II), 4. Ni(II), 5. Cu(II) fibers.

There were broad peaks having maximum at $2\theta = 10^\circ$ corresponding to 0.88 nm interplanar distance for all fibers except Co(II) fibers.

Despite it was not possible to observe all expected X-ray diffraction peaks of these materials in X-ray diagram due to their imperfect crystal formations, it is clear that all of the fibers were mixtures of hydrated silicates, carbonates, hydroxides or soluble salts.

Analysis of Water Vapor and N_2 Adsorption

The fibers were outgassed at 150°C temperature which was just sufficient to remove all free water from their pores prior to adsorption experiments. N_2 adsorption was done at 77 K and it was physical adsorption. H_2O adsorption was carried out at 25°C and functional groups that make hydrogen bond with water were required on the surface of the fibers for water vapor adsorption. All fibers had water chemically bound to their structure as indicated by their TGA curves and no Si-OH groups as seen in their IR spectra. Adsorption isotherms for N_2 and H_2O on the fibers are seen in Figs. 7 and 8. Lower amounts of N_2 was adsorbed than H_2O in the low-pressure range. Similar behavior was observed for precipitated silica, which had both micropores and mesopores [20]. This could be due to

i. Ability of the small molecules of H_2O with 0.28 nm diameter to enter into pores where N_2 molecules with 0.33 nm diameter were excluded due to their larger size or
ii. Adsorption of water vapor on the fiber surface through hydrogen bonding.

If the first case was considered, Dubinin Asthokov (D.A) equation given below based on the volume filling theory of micropores [21] could be applied to H_2O adsorption data.

$$V = V_o \exp(-A/\beta E_o)^n \qquad (6)$$

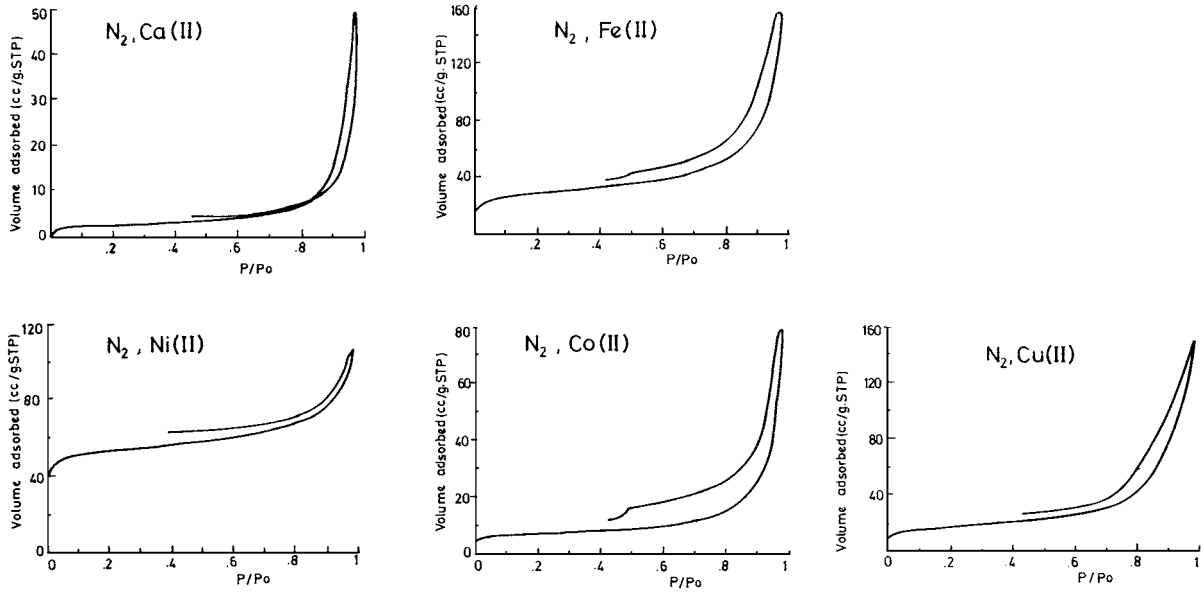

Figure 7. N_2 adsorption isotherms at 77 K.

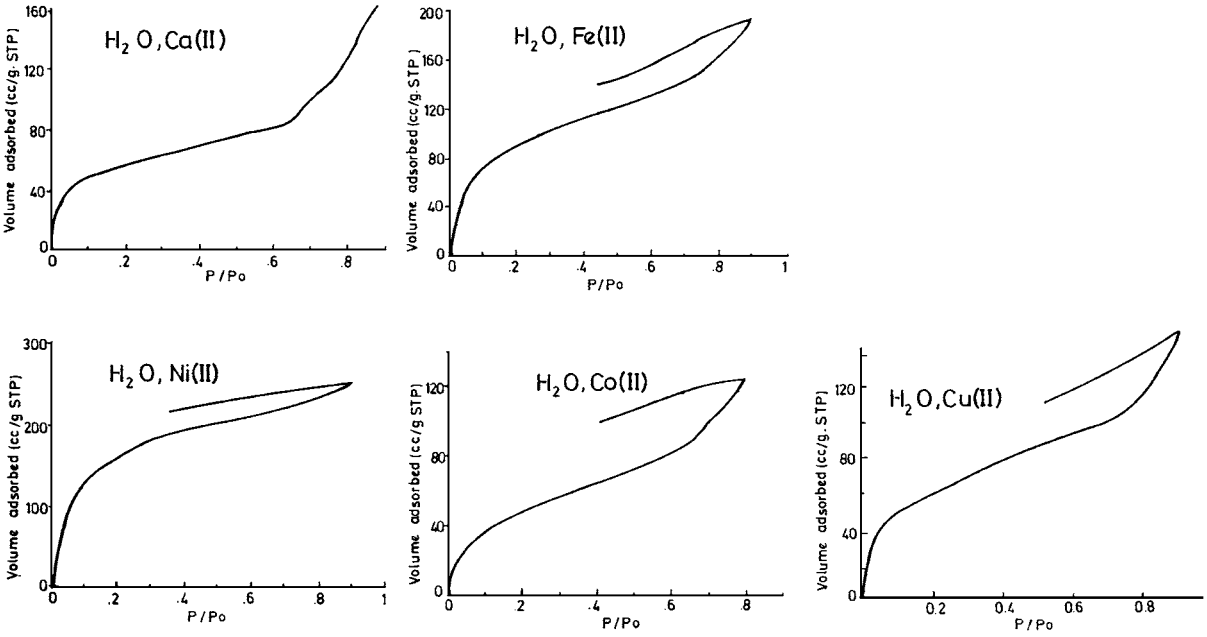

Figure 8. H_2O adsorption isotherms at 25°C.

Where $A = RT\,lnP^{o}/P$, $R =$ universal gas constant, $T =$ absolute temperature, $V_o =$ micropore volume, $V =$ volume adsorbed at relative humidity P/P^{o}, $E_o =$ characteristic energy of reference adsorbate benzene, $\beta =$ similarity coefficient to reference adsorbate benzene.

By taking the natural logarithm of Eq. (6) twice

$$lnln(V_0/V) = n\,lnA - n\,ln(\beta E_o) \qquad (7)$$

is found. The plot of $lnln(V_0/V)$ versus lnA has slope n and intercept $-n\,ln(\beta E_o)$. The values for n, V_o and pore

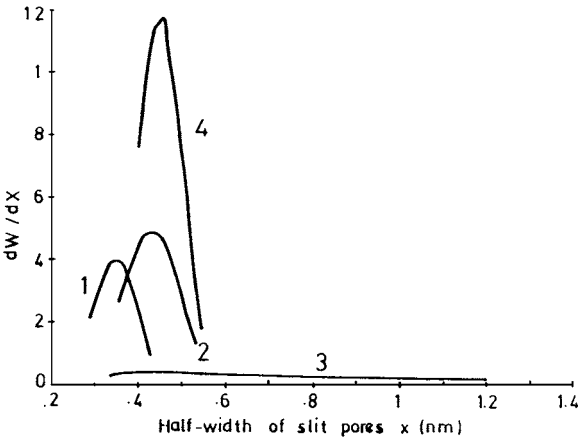

Figure 9. Micro pore size distribution from D. A. equation. 1: Cu(II), 2: Fe(II), 3: Cu(II), 4: Ni(II).

width were calculated using the software of Omnisorb 100CX and reported in Table 2. β was taken as 0.2 for water vapour. Solutions of D-A model could be obtained for all fibers except Co(II) case. The value for n is very close to 2 for all fibers indicating Dubinin Raduskevitch equation, which is the special case of Dubinin Asthokov equation was followed by the samples [21]. The D-A pore size distribution seen in Fig. 9 showed average micro pore radius of the fibers were 0.34–0.46 nm range which corresponds to 0.68 to 0.92 nm pore size which was at the same order of interplanar spacings observed at 0.88 nm ($2\theta = 10^\circ$) for Fe(II) Ni(II) and Cu(II) fibers. X-ray diffraction did not indicate presence of interplanar spacings of around 0.88 nm and adsorption on Co(II) fibers did not fit to D-A model. In other words Co(II) fibers did not have micropores. The micropore size found from D-A model was much larger than the size of N_2 molecules. Thus the higher adsorption of H_2O than N_2 in the low pressure region could not be only due to the difference in size of two molecules, it should also be due to hydrogen bonding of H_2O to the fibers. This was also confirmed by hysteresis on water vapor adsorption. Adsorbed water could not be completely desorbed from the fibers unless they were heated at high temperatures as indicated by TGA analysis.

Surface area from N_2 adsorption data was in the range of 10–249 $m^3\ g^{-1}$ and 8–176 $m^2\ g^{-1}$ from Langmuir and B.E.T models respectively as seen in Table 3. The total pore volume was 0.08–0.24 $cm^3\ g^{-1}$ from N_2 adsorption. D-A micropore volume was found in between 0.05–0.15 $cm^3\ g^{-1}$ from H_2O adsorption data.

All the samples had meso pores causing capillary condensation of the adsorbates. The pore size distribution of the fibers in the mesopore range shown in Fig. 10 was found from Kelvin equation [21] using nitrogen desorption data. The maximum population was at 4 nm for Ni(II) and Cu(II) fibers.

Hysteresis was observed both for N_2 and H_2O adsorption due to capillary condensation as seen in Figs. 7 and 8. H_2O desorption was less complete than N_2 adsorption at relative pressure 0.4 due to hydrogen bonding of water vapour on the surface of silica.

Influence of Metal Ion on Properties of the Fibers

The solubility of metal hydroxides in water affected the metal content of chemical garden fibers. When the fibers were arranged in increasing order of M(II) content as in Table 4, correlation between its properties and the solubility product of hydroxides were observed. The most soluble hydroxide in this study was $Ca(OH)_2$ and Ca(II) fibers had the lowest M(II) content. The Cu(II) content of Cu(II) fibers was also low even though

Table 3. Adsorption characteristics of hollow fibers.

		Fiber type				
Adsorption characteristics	Adsorbate	Ca(II)	Fe(II)	Co(II)	Ni(II)	Cu(II)
Total pore volume ($cm^3\ g^{-1}$)	N_2	0.08	0.24	0.12	0.15	0.23
	H_2O	0.12	0.15	0.10	0.2	0.12
D-A micropore volume ($cm^3\ g^{-1}$)	H_2O	0.05	0.09	–	0.15	0.06
D-A micropore radius (nm)	H_2O	0.34 ± 0.05	0.42 ± 0.07	–	0.44 ± 0.05	0.46 ± 0.29
D-A "n" value	H_2O	1.94	2.00	–	2.02	1.93
Surface area (m^2/g)	N_2, BET	8	96	24	176	60
	N_2, Langmuir	10	135	33	249	85
	H_2O, BET	81	221	124	283	107

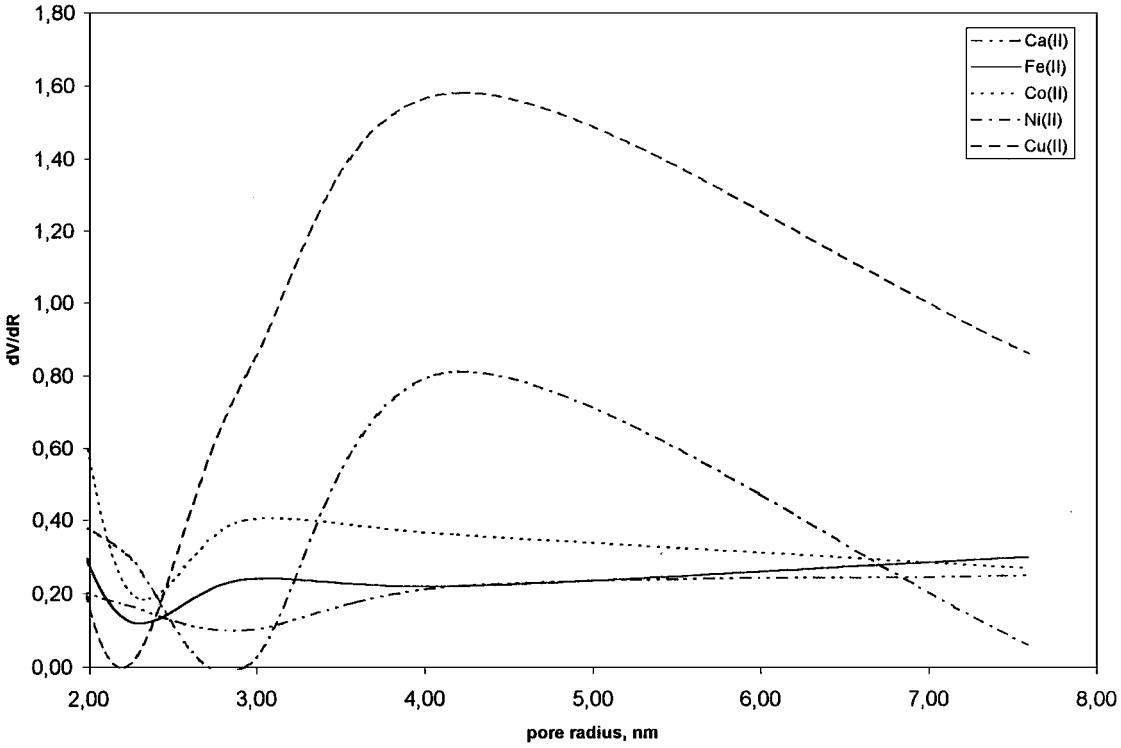

Figure 10. Meso pore size distribution from Kelvin equation.

the solubility of $Cu(OH)_2$ was very low. This indicated that the metal content was not controlled solely by the metal hydroxide solubility.

The IR spectroscopy also indicated Si-O vibration of SiO_2 at 1090 cm^{-1} were dominant for Ca(II) and Cu(II) fibers due to their higher SiO_2 content. The Co(II), Ni(II), Fe(II) fibers with higher M(II) content had M-O stretching vibration at 1040 cm^{-1}.

The surface area of the fibers were also increased with increase in metal (II) content as seen in Table 4. Since the fibers had SiO_2 at their outer surface and metal oxide in their inner surface, their surface area should be both effected from the particle size of their components. Elementary particle size of SiO_2 depends on the pH of the gelation medium. SiO_2 gelled in basic and acidic medium had low and high surface area respectively. Since large elementary particles formed at basic pH values outside the fibers their surface area should be low [3]. The metal oxide particles formed at the inner surface could have smaller size due to nucleation effect of metal silicate membrane formed between water glass and metal salt solution and thus have larger surface area.

Table 4. Influence of metal hydroxide solubility on properties of the fibers.

	Mols M(II)/mols SiO_2	Solubility product of M(II) hydroxide	Density g/cm^3	Surface area, g/m^2	Si-O or M-O stretching frequency
Ca(II)	0.31	2.4×10^{-6}	2.5	8	1040
Cu(II)	0.46	5.6×10^{-20}	2.8	60	1040
Co(II)	0.65	1.4×10^{-15}	5.0	24	1090
Ni(II)	0.71	9.1×10^{-14}	5.2	176	1090
Fe(II)	1.06	2.0×10^{-24}	3.6	135	1090

The densities of the fibers reported in Table 4 as being in the range 2.5 to 5.2 g/cm^{-3} were also increased with metal (II) content except Fe(II) fibers. The existance of closed pores in the fibers effecting their densities should also be taken into consideration.

Conclusion

Quantitative data were obtained about morphology, chemical composition and surface characteristics of the chemical garden fibers. Dried fibers were hollow and had very smooth external and globular internal

surfaces. The hollow metal silicate fibers formed without any extrusion [10] or templating [8, 9] process in chemical gardens. On the other hand they were very fragile and broken during handling. The attempt to strengthen them by wet aging failed because of silica hydrogel formation outside the fibers. They had variable composition with metal (II) oxide/SiO_2 ratio being in the range of 0.31–1.02. X-ray diffraction indicated amorphous structures for Fe(II), Co(II) and Ni(II) fibers and presence of crystalline $CaCO_3$, $CaO{\cdot}SiO_2{\cdot}H_2O$ and hydrated double sodium calcium silicate phases in Ca(II) fibers and $CuO{\cdot}SiO_2{\cdot}H_2O$ and $CuSO_4$ hydrates in Cu(II) fibers. Non of the fibers contained only one substance, they were mainly mixtures of metal silicate hydrates, silica, metal oxide hydrates and had small amounts of carbonates or sulfates. While Fe(II), Co(II) and Ni(II) fibers were amorphous, Ca(II) and Cu(II) fibers had crystalline structure. Fibers containing hydroxides with high solubility in water contained less metal ions. All the fibers except Co(II) had bi disperse pore size distribution. They had pores both in micro porous and meso porous region. The B.E.T surface area from N_2 adsorption data was in the range of 10–249 $m^3\ g^{-1}$ and 8–176 $m^2\ g^{-1}$ from Langmuir and B.E.T models respectively. The total pore volume was 0.08–0.24 $cm^3\ g^{-1}$ from N_2 adsorption. D-A model showed the fibers had 0.05–0.15 $cm^3\ g^{-1}$ micropore volume from H_2O adsorption data.

References

1. R.J. Gillespie, D.A. Humpreys, N.C. Baird, and E.A. Robinson, *Chemistry* (Allyn and Bacon, Boston, 1986).
2. H.W. Roesky and K. Möckel, *Chemical Curiosities* (VCH Weinheim, New York, 1996).
3. R. K. Iler, *The Chemistry of Silica* (John Wiley, New York, 1979).
4. R.D. Coatman, N.L. Thomas, and D.D. Double, J. Mat. Sci. **15**, 2017 (1980).
5. C. Collins, W. Zhou, A.L. Mackay, and J. Klinowski, Chem. Phy. Letters **286**, 88 (1998).
6. C. Collins, G. Mann, E. Hope, T. Duggal, T.L. Barr, and J. Klinowski, Phy. Chem. Chem. Phy. **15**, 3685 (1999).
7. M. Atik and J. Zarzycki, J. Mat. Sci. Let. **8**, 32 (1989).
8. H.P. Lin, S. Cjeng, and C.Y. Mou, Chem. Mater **10**, 581 (1998).
9. V. Valtchev, B.J. Schoeman, J. Hedlund, S. Mintova, and J. Sterte, Zeolites **17**, 408 (1996).
10. US patent no. 5547263 (1966).
11. X. Feng, C.Y. Pan, C.W. McMinis, J. Ivory, and D. Gosh, AIChE Journal **44** , 1555 (1998).
12. D. Balköse, F. Özkan, U. Köktürk, and S. Ulutan, *Silica 98*, Extended Abstracts (Univ. Heute Alsace, Mulhouse,1998), p. 79.
13. J.E. Schenk and W.J. Weber, AWWWA 199 (1968).
14. K. Tsukioka, Asahi Garasu Kenkyu Hokoku **5**, 163 (1965) in *Silicate Science*, edited by W. Eithel (Academic Press , New York, 1966).
15. G.D. Knowlton and T.R. White, Clays and Clay Minerals **29**, 403 (1981).
16. J. Goworek and W. Stefaniac, Mat. Chem. Phys. **32**, 244 (1992).
17. M.N. Ackerman, Chemical Education **47**, 70 (1970).
18. H. Baltacioğlu and D. Balköse, Ege Univ. Fac. Eng. J. C **5**(1), 29 (1988).
19. E.W. White and G.G. Johnson, *ASTM Data Series* (Philadelphia, 1970).
20. P.W. Stainer, C.R. Owen, and I.P. Mckeon, *Silica 98*, Extended Abstracts (Univ. Heute Alsace, Mulhouse, 1998), p. 821.
21. S.J. Gregg and K.S.W. Sing, *Adsorption, Surface Area and Porosity* (Academic Press, London, 1982).